ACS APPLIED MATERIALS & INTERFACES

Research Article

www.acsami.org

Dye-Sensitized Nanoarrays with Discotic Liquid Crystals as Interlayer for High-Efficiency Inverted Polymer Solar Cells

Yueqin Shi,[†] Licheng Tan,[†,‡] and Yiwang Chen*[,†,‡]

[†]Institute of Polymers/College of Chemistry, Nanchang University, 999 Xuefu Avenue, Nanchang 330031, China

[‡]Jiangxi Provincial Key Laboratory of New Energy Chemistry, Nanchang University, 999 Xuefu Avenue, Nanchang 330031, China

Supporting Information

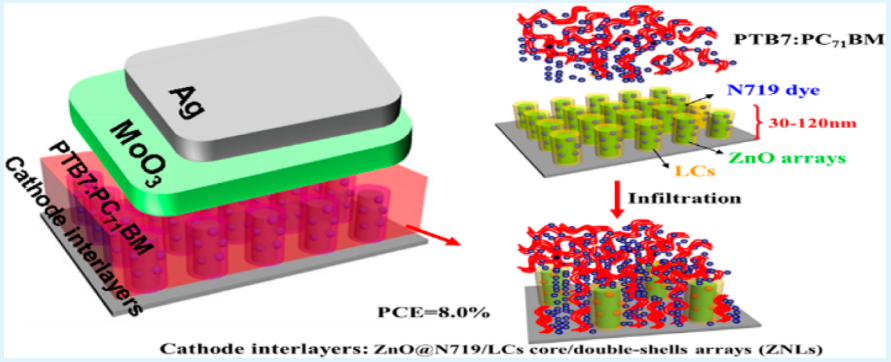

ABSTRACT: The well-aligned and highly uniform one-dimensional ZnO with organic dyes core/shell (ZNs) and ZnO with dyes and liquid crystals core/double-shells nanoarrays (ZNLs) with controllable lengths were fabricated as electron transport layers (ETLs) in inverted polymer solar cells (PSCs). Ditetrabutylammonium cis-bis(isothiocyanato)bis(2,2′-bipyridyl-4,4′-dicarboxylato) ruthenium(II) dye (N719) was presented to reduce the surface defects of ZnO nanoarrays (NAs). In addition, the shell modification could decrease the electron injection barrier between ZnO and active layer, thereby facilitating electron injection effectively and forming a direct electron transport channel into the cathode. Due to the orientation of nanoarrays and the self-organization of 3,6,7,10,11-pentakis(hexyloxy)-2-hydroxytriphenylene liquid crystals (LCs) in liquid crystalline mesophase and isotropic phase transition, the components of active layer would be driven rearrange and infiltrate among the interspaces of nanoarrays more orderly. The increased interfacial contact between cathode and active layer would benefit charge generation, transportation and collection. On the basis of these advantages, it was found the N719 shell and N719/LCs double-shells modifications of ZnO NAs could boost the photovoltaic performance of PSCs with the best power conversion efficiency (PCE) of 7.3% and 8.0%, respectively.

KEYWORDS: *nanoarrays, core/double-shells, liquid crystals, polymer solar cells*

INTRODUCTION

Extensive efforts have been directed at developing polymer solar cells (PSCs) because of their potential advantages for lightweight, low-cost energy harvesting and flexibility.[1,2] Material interfaces of electron donor (D) and acceptor (A) in PSCs are very important. Photoinduced charge generation and recombination, which is the major charge loss mechanism, mainly take place at this interface.[3] Therefore, modifying the D/A interface could significantly improve the performance of PSCs. In addition to the morphology optimization and new materials design of active layer, interlayers play a crucial role in transporting charge carriers from the active layer to the corresponding electrodes and preventing interfacial charge recombination, and subsequent enhancing the power conversion efficiency (PCE) and stability of device. To improve the charge selectivity and, at the same time minimize the energy barrier for charge extraction at electrodes, a hole transporting layer (HTL) with electron-blocking properties is inserted between the anode and active layer, and an electron transporting layer (ETL) with hole-blocking properties is inserted between the cathode and active layer. Besides, roll-to-roll solution processing of PSCs is widely considered as a key technology toward commercialization of photovoltaic devices.

To fabricate the ETL, researchers have commonly utilized the solution-processed n-type metal oxides in inverted PSCs (i-PSCs) to modify the cathode electrode.[4−6] Through interfacial engineering of a solution-processed electron extraction layer to facilitate electron transport and suppress bimolecular recombination, the high PCE could be obtained.[7−10] In particular, zinc oxide nanoparticles (ZnO NPs) are used as the ETL because of their low work function (WF), ease of synthesis and good optical transparency, as well as high electron mobility.

Received: July 10, 2014
Accepted: September 30, 2014
Published: September 30, 2014

ACS Publications © 2014 American Chemical Society

Scheme 1. Molecular Structures of N719, LC Small Molecules, and Active Layer Materials, and the Device Structure of Polymer Solar Cells by Utilizing the ZnO@N719 Core/Shell Nanoarrays (ZNs) and ZnO@N719/LCs Core/Double-Shell Nanoarrays (ZNLs) as Electron Transport Layers

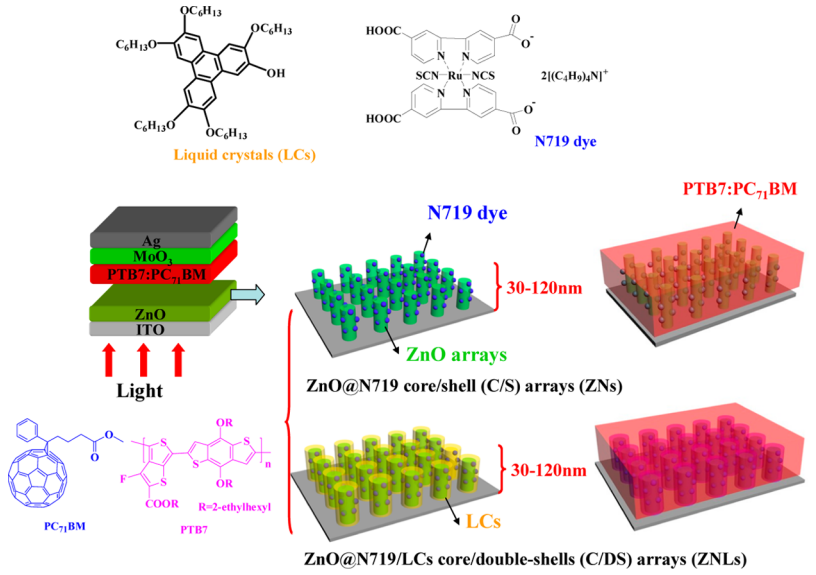

However, the major challenges in using ZnO NPs as ETL are the presence of surface defects with adsorbed oxygen[11] and the poor spatial distribution of the NPs over a large area.[12,13] Accordingly, there are many needs to develop low-defect and uniformly oriented nanostructures of ZnO films as ETL to realize high efficiency of i-PSCs. On the other hand, the inorganic electron-collecting interlayer has poor interfacial contact with the organic active layer, which could result in poor electron extraction, and thus interfacial modification between ZnO and active layer has also became an important issue for improving the photovoltaic performance of i-PSCs.

One-dimensional nanostructure of ZnO is a wise choice as ETL to provide the directionality of electrons' migration in i-PSCs.[14−17] Moreover, the well-oriented and aligned ZnO nanoarrays (NAs) has grown successfully regardless of the pattern of the substrate, disordered or oriented initial seed layer, even on amorphous glass.[18] It was reported that the oriented ZnO NAs grew on different types of substrates with various degrees of crystallinity of ZnO, and showed they were still able to form well-aligned and oriented ZnO NAs.[19]

To passivate the surface defects of ZnO NAs and eliminate the poor interfacial contact between inorganic electron-collecting interlayer and organic active layer, the interface modification of ZnO NAs with organic materials could be an important approach for achieving maximum efficiency in i-PSCs.[20,21] A surface-modified ZnO-poly(vinylpyrrolidone) (PVP) composites as ETL between active layer and cathode had been reported to promote the charge collection and PCE of device in i-PSCs.[11] It was also proposed that a fullerene derivative (PCBE−OH)-doped ZnO as the cathode could be effective for the collection of electrons to enhance the photovoltaic performance of device.[5] Besides, the excellent performance was exhibited in a photovoltaic device with silicon nanowire array/carbon quantum dot core−shell heterojunction because of the optimized carrier transfer and collection capability, as well as the improved optical absorption.[22]

In addition, to promote the permeation of active layer components into the ZnO NAs, and meanwhile, to drive the self-assembly of active layer materials without additional external treatments, the small molecule liquid crystals are considered. The organization of liquid crystals could induce the molecular rearrangement of active layer directly originating from the liquid-crystalline ordering and elastic deformation upon the phase transition of liquid crystallines.[23,24] It has been demonstrated that liquid crystalline organization of diketopyrrolopyrrole (DPP)-based mesomorphic small molecule materials could tune the morphology of active layer and improve the photovoltaic performances of devices.[25]

Herein, we report a novel method to enhance the charge collection in i-PSCs using solution processed ZnO with organic dyes core/shell nanoarrays (ZNs) and ZnO with dyes and liquid crystals core/double-shells nanoarrays (ZNLs) as ETL, respectively. The N719 is ditetrabutylammonium cis-bis-(isothiocyanato) bis(2,2′-bipyridyl-4,4′- dicarboxylato) ruthenium(II) dye, and LCs is 3,6,7,10,11-pentakis-(hexyloxy)−2-hydroxytriphenylene liquid crystalline small molecule. This pathway for the formation of one-dimensional core/double-shells nanostructures has not been explored so far, and may be supposed the first step in the development of high efficiency solution-processed i-PSCs with core/double-shells nanoarrays interlayers and to realize the commercialization of photovoltaic devices.

RESULTS AND DISCUSSIONS

The PCE of solution-processed i-PSCs in Scheme 1 could be optimized significantly by inserting the optical spacer nanoarrays between the active layer and ITO electrode. The ZnO NA, ZN, and ZNLs with controllable lengths were first synthesized, and then, the components of active layer were filled among the nanoarrays. Thus, optimum performances of the devices could be obtained by combination of the modifications of conjugated shell and double-shells nanostructures, where the ZnO NA, ZN, and ZNL layers for blocking holes were used to improve the light-harvesting and increase the charge collection efficiency. The enhancement of light absorption of the cells was testified by the external quantum efficiency (EQE) and UV−vis absorption spectroscopy measurements. The surface defects of ZnO NA core could be

restrained by the formation of organic N719 shell or N719/LCs double-shells. Besides, the molecular self-assembly of active layer components could be driven by the orientation of core/shells nanoarrays and reorganization of LC molecules. The improvements of combined optical and electrical properties could raise the PCE of solution-processed i-PSCs up to an average of 7.8%.

Characterization of the ZnO NPs, ZnO NAs, ZNs and ZNLs crystal nanostructures by transmission electron microscopy (TEM) was processed in Figure S1. The ZnO NPs initial seed layer of ∼5 nm in diameter with well dispersion was formed, and one-dimensional ZnO NAs, ZNs, and ZNLs with highly orientation had been successfully synthesized on the ITO substrates. To further investigate the nanostructures of ZnO NPs, ZnO NAs, ZNs, and ZNLs, the high-resolution transmission electron microscopy (HRTEM) mode was acquired in Figure 1. The lattice spacing of about 0.25 nm belonging to the

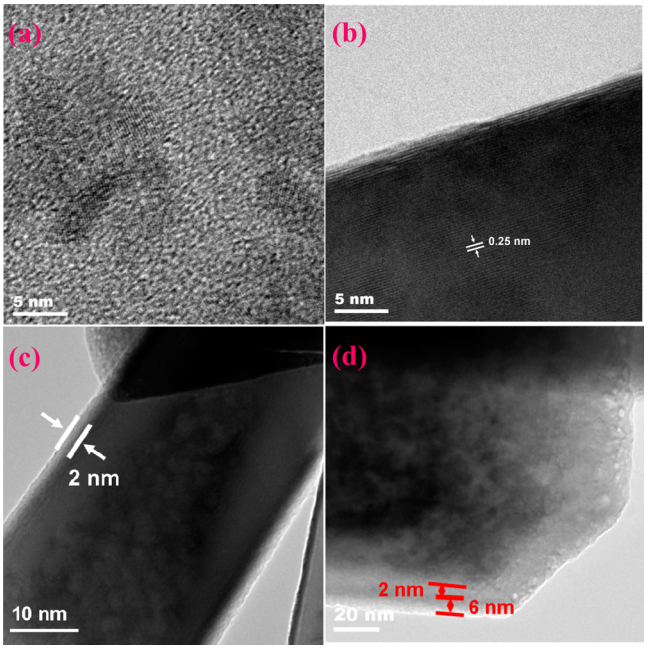

Figure 1. High-resolution transmission electron microscopy (HRTEM) of (a) ZnO NPs, (b) ZnO NAs, (c) ZNs, and (d) ZNLs.

(002) plane of hexagonal ZnO NAs and the ZnO NAs on the order of 40−50 nm in diameter were observed. From Figure 1, compared with the pristine ZnO NAs, the N719 organic shell and N719/LCs homogeneous double-shells covered the 1D nanostructure ZnO NAs fully, which showed the thicknesses of N719 shell and LCs shell were ∼2 and 6 nm, respectively. The TEM data confirmed that the formation of the organic shell or double-shells onto the ZnO NA surface completely.

Top view scanning electron microscopy (SEM) images of ZnO NA films grown with various lengths were displayed in Figure S2 in the Supporting Information. At 0 min, the thickness of ZnO NPs seed layer with highly density distribution was approximate 30 nm measured by tapping-mode atomic force microscopy (AFM). With longer growth time, the crystallites of ZnO began to present nanowire structures (ZnO NAs), first with needlelike ends and developing very slowly, then forming hexagonal tops and progressing relatively quickly, and finally stopping growth over 3 μm. As the growth nutrients were being consumed, the nanoarrays' growth of ZnO was suspected to level off, similar to ref 18. The density of ZnO NAs drastically diminished and then almost remained unchanged upon a certain length. Besides, the graphical representation of thickness with growth time was indicative of the *c*-axis peak first with the low growth rate and then a rapid growth rate during 0−150 min (see Figure S3 in the Supporting Information). And the detailed relationship between the number of surviving crystals and the distance from the growth substrate was illuminated as ref 18. To further testify the selective growth direction of ZnO NAs, the XRD data of ZnO NP, ZnO NA, ZN, and ZNL samples are displayed in Figure S4 in the Supporting Information. Compared with pristine ZnO NPs film, the *c*-axis peaks of ZnO NA, ZN, and ZNL films with the optimal orientation were all generated, where the *c*-axis is normal to the substrate, in agreement with the following SEM data.

Although the ZnO NAs possessed many advantages, such as relative low WF, high optical transparency, and electron mobility, it was still challenge for ZnO NAs as ETL in i-PSCs to achieve high efficiency due to the presence of poor interfacial contact with organic active layer and defects with absorbed oxygen.[26−28] Hence, the N719 shell and N719/LCs double-shells were introduced to modify the interface between the organic active layer and ZnO NAs, and passivate the surface defects of ZnO NAs. The surface morphologies of ZNs with various thicknesses were displayed by conducting AFM measurement in Figure 2. The well-dispersed morphology

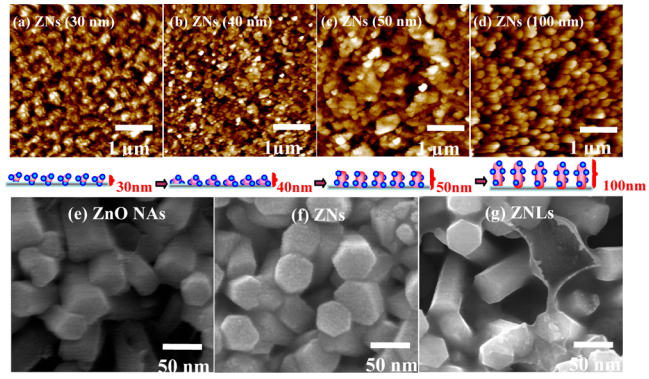

Figure 2. Tapping-mode AFM images of ZNs thin films with various thicknesses: (a) 30, (b) 40, (c) 50, and (d) 100 nm. The below insets showed the corresponding illustration describing the thicknesses of ZNs over growth time of ZnO NAs. Top SEM views of (e) ZnO NAs, (f) ZNs, and (g) ZNLs.

was observed in film of ZNs. With the thickness of ETL increasing, the ZNs grew perpendicularly to the substrates, first with needlelike top and then with columnar-like ends, consistent with the results of Figure S2 in the Supporting Information. To gain further insight into the nanomorphology of ZNs and ZNLs clearly, the SEM with high magnification was tested. The hexagonal columnar nanostructure of ZnO NAs with a length of 40−60 nm was formed. After the N719 spin-coating onto the ZnO NA surface, the morphology of original nanoarrays was not altered remarkably and simultaneously, a core/shell nanostructure could be fabricated with the dense nanoclusters of N719 covering onto ZnO NAs clearly. Moreover, a core/double-shell nanomorphology with the fluidlike shell as surface modification could be obtained upon the LCs coating onto the ZNs, originating from the self-organization of liquid crystalline mesophase and isotropic phase

transition. Besides, it is well-known that the surface defects and crystal quality of ZnO could be optimized through surface modification, ascribing to the amphiphilic property of N719 and LCs, which could form the better electronic coupling between the cathode interlayers and $PC_{71}BM$ or $PC_{61}BM$ acceptor of the active layer.[29−31] The optical properties of ZnO NPs, ZnO NA, ZN, and ZNL films were also measured by UV−vis absorption in Figure S4 in the Supporting Information. With respect to ZnO NPs film, the absorption of films with nanoarrays all demonstrated a red-shift because of the growth of the ZnO crystals with optimal orientation.[32−34]

To investigate the infiltration of the components of active layer into ZNs, we carried out SEM with the top and cross-section. First, P3HT:$PC_{61}BM$ was chosen as the active layer to explore the immergence of components among the nanoarrays. Figure 3 revealed the P3HT:$PC_{61}BM$ active layer materials

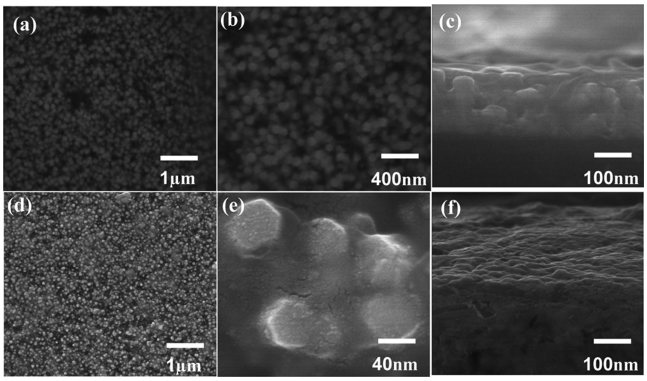

Figure 3. (a) Top-view, (b) high-resolution, and (c) cross-section SEM images of P3HT:$PC_{61}BM$ active layer spin-coating onto ZNs surface without thermal annealing, and (d) top,view, (e) high,-resolution, and (f) cross-section SEM images of P3HT:$PC_{61}BM$ active layer spin-coating onto ZNs surface with thermal annealing at 150 °C.

could infiltrate into the interspaces, especially for the film with thermal annealing at 150 °C for 30 min. For an efficient device of i-PSCs, the components of active layer should simultaneously be formed with bicontinuous D and A networks, optimal D/A interfacial area for efficient charge separation, and finally, domain sizes on the scale of a few tens of nanometers to match the exciton diffusion lengths of ∼10 nm. Because of the vertical orientation structure of nanoarrays and the space among nanoarrays controlled in tens of nanometer observing from the top views of SEM, the components of active layers could be directed to phase-separate into nanoscale and form an ideal morphology to promote the charge generation, separation and transmission. On the other hand, from the results of UV−vis absorption spectra (see Figure S5 in the Supporting Information), the absorption peaks of films with P3HT:$PC_{61}BM$ spin-coating onto the ZNs surface were red-shifted with approximate 15 nm, probably attributing to the self-assembly and orientation of P3HT chains of active layer with an enhancing planarity of the packed conjugated polymer chains, respect to the film of ZnO NPs. After thermal annealing, the peak at 610 nm reduced, revealing the weaker intermolecular interaction of P3HT with $\pi-\pi$ stacking because of the infiltration of active layer components into ZNs.

The successful coverage of N719 single shell and N719/LCs double-shells onto the ZnO NA surface was confirmed by X-ray photoelectron spectroscopy (XPS), and the core-level XPS spectra for C 1s, O 1s, N 1s, and Zn 2p of ZnO NA, ZN, and ZNL films are shown in Figure 4. After spin-coating the single N719 shell and N719/LCs double-shells onto ZnO NAs, the relative magnitude of O 1s peak at 531.4 eV corresponding to the oxygen atoms bonded to the zinc in the ZnO matrix was increased about 50%. Thus, the number of Zn−O bonds at the surface in the wurtzite structure of ZnO NAs was enhanced. The interfacial modification decreased the relative magnitude of the peak at ∼530.0 eV, which corresponds to O^{2-} ions presenting in the porous ZnO clusters, but not chemically bonding to zinc in the ZnO structure. Besides, the ZNs and ZNLs displayed declining peaks rapidly for Zn 2p at 1020.9 and 1021.3 eV, corresponding to the Zn−O bonds, and red-shifted after modifying with the small molecules, comparing to the

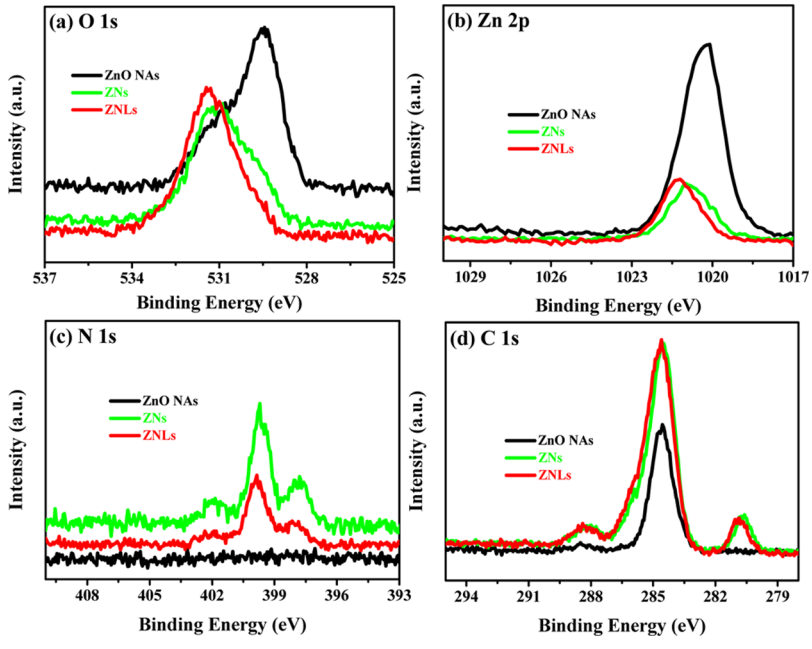

Figure 4. (a) O 1s, (b) Zn 2p, (c) N 1s, and (d) C 1s of XPS data for the as-prepared ZnO NA, ZN, and ZNL films.

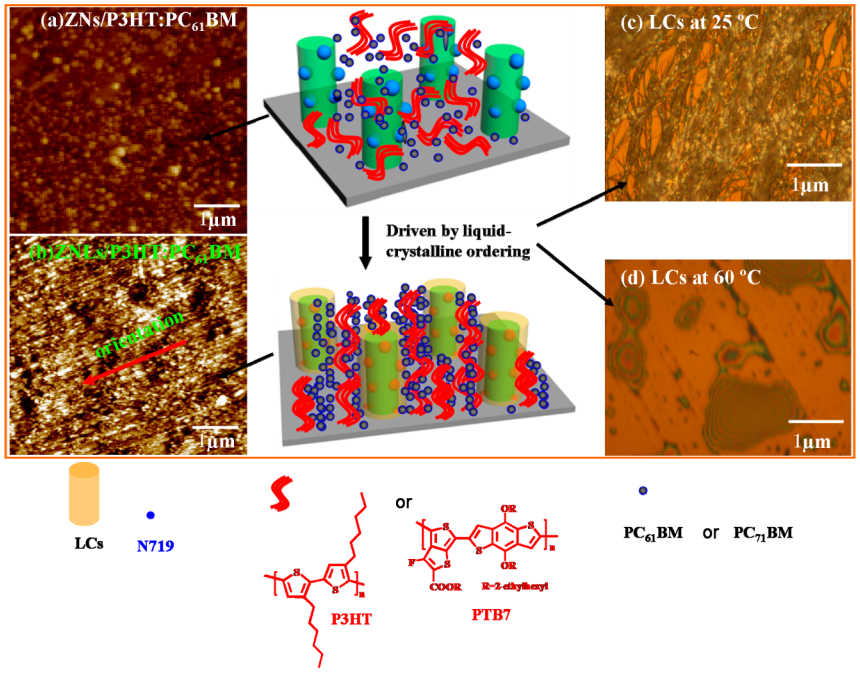

Figure 5. AFM height images (left) of P3HT:$PC_{61}BM$ spin-coating onto (a) ZNs and (b) ZNLs surface. Polarizing optical micrography (POM) (right) of LCs small molecule (c) at 25 °C and (d) 60 °C. The schematic images (middle) displayed the self-assembly of active layer driven by the liquid crystalline ordering, with the corresponding components below.

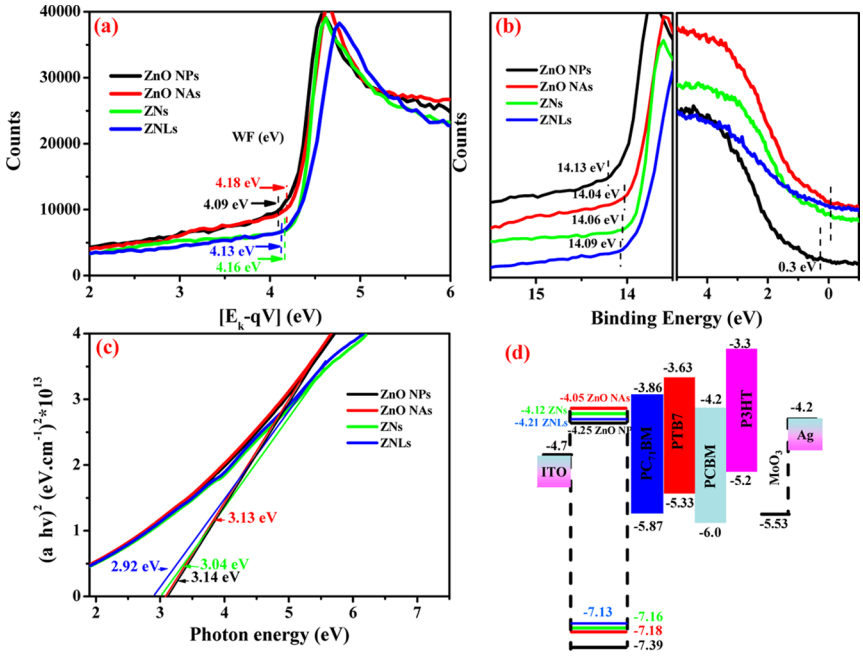

Figure 6. UPS results of ZnO NPs, ZnO NAs, ZNs, and ZNLs with (a) the work functions and (b) its corresponding high binding energy cutoff and HOMO region. (c) Optical band gap energy of ZnO NPs, ZnO NAs, ZNs, and ZNLs. (d) Electron structures of the materials used in the devices of PSCs.

ZnO NA film showing the Zn 2p peak at 1020.3 eV. The corresponding N 1s and C 1s peaks for the ZNs and ZNLs films all demonstrated higher energy values, especially for the ZNs film.On the basis of the XPS data, good coverage of N719 shell and N719/LCs double-shells on the surface of ZnO NAs was realized.

The thermotropic liquid crystalline behavior, relative to the molecular assembly and optoelectronic properties of LCs, was investigated by temperature-controlled polarizing optical micrography (POM) in Figure 5.[23,25] All the mesophases of LCs showed fibrous-shaped textures of smectic phases, and the sizes of domains were large about several tens of nanometers, respectively. And then a scattered stack of plate-shaped texture was turned after thermal annealing at 60 °C with sizes over several micrometers. Further heating over 80 °C led to disappearance of the birefringence, corresponding to the transition into isotropic liquid phase. In addition, after the temperature dropping to below 50 °C, the obvious trend of

Table 1. Device Parameters of PTB7:$PC_{71}BM$ Solar Cells with Different Cathode Interfacial Layers under the Illumination of AM 1.5G, 100 mW/cm^2

device[a,b]	J_{sc} (mA/cm^2)	V_{oc} (V)	FF (%)	PCE (%)	R_s(Ω cm^2)	R_{sh} (Ω cm^2)
ITO/ZnO NPs/PTP[c]/MoO_3/Ag	13.7	0.73	65	6.5 ± 0.2	1.19	450.7
ITO/ZnO NAs/PTP[c]/MoO_3/Ag	16.0	0.72	53	6.1 ± 0.3	5.2	335.1
ITO/ZNs/PTP[c]/MoO_3/Ag	16.5	0.73	58	7.0 ± 0.2	5.4	241.0
ITO/ZNLs/PTP[c]/MoO_3/Ag	16.4	0.73	65	7.8 ± 0.2 (8.0)[d]	2.3	462.0

[a]All values represented averages from 0.0418 cm^2 devices on a single chip. And all data of devices had been tested from more than five substrates (15 chips) to ensure reproducibility. [b]Device structure: ITO/interfacial layers/active layer/Ag (8.0 nm MoO_3). [c]PTP represented PTB7:$PC_{71}BM$ (1:1.5 w/w). [d]Respected the best PCE of device.

such stack of plate morphology driven by liquid crytalline organization was observed again. To gain deeper insight into the effect of variation by liquid crytalline organization properties on P3HT:$PC_{61}BM$ nanostructures, the morphology of active layer had been analyzed using UV−vis absorption and AFM measurements. Compared with the film of P3HT:$PC_{61}BM$ casting onto ZNs surface, the absorption spectra of film with LCs modification showed red-shifted obviously in Figure S6 in the Supporting Information, indicating the conjugated polymer main chains of P3HT in active layer had assembled into more planar nanostructures with highly orientation.[35,36] The film of P3HT:$PC_{61}BM$ covering onto ZNs surface with thermal annealing treatment demonstrated a well phase-separated morphology in the images of AFM. The obvious trend of orientation and self-assembly of morphologies' changes by liquid crytalline organization was observed in the film with the modification of LCs, ascribing to the organization of mesogenic phase after the thermal annealing and the strengthened interactions among conjugated polymer main chains. The detailed morphological change of active layer by liquid crytalline organization was revealed in the schematic diagram. We clarified that self-assembly of LCs with thermal annealing measurement allowed the active layer to reorganize and diffuse into thermodynamically favorable interpenetrating networks in nanoscale,[37,38] which could be beneficial to effective exciton dissociation and charge transport in the active layer of i-PSCs.

The primary requirement of interlayers lay in their ability to produce large interfacial dipoles and modify the WF of the cathode electrode, and consequence increase the electron injection into cathode electrode.[39] To verify the effects of N719 shell and N719/LCs double-shells interface modifiers on ZnO NA thin layer's interfacial dipoles, UPS (Figure 6) was carried out to study the WF[40,41] and energy levels of ZnO NPs, ZnO NA, ZN, and ZNL films. Comparing to the ZnO NPs film, the higher WF values of devices with ZnO NAs was illustrated. After interfacial modifications of ZnO NAs, ZNs (approximately −4.16 eV) and ZNLs (approximately −4.13 eV) all shifted the WF of ZnO NAs (approximately −4.18 eV) with lower values because of the interfacial dipole induced by the large number of polar groups in their structure of N719 and LCs (Scheme 1). The relative low WF of ZNs and ZNLs allowed them to form better ohmic contacts with cathode and increased the built-in field to break the electrical symmetry inside of the cells, which was beneficial to enhance charge extraction and reduce recombination losses. In addition, the large V_{oc} from the inverted PSCs were anticipated for the lower WF of ZnO NAs with the interfacial modifications of N719 shell and N719/LCs double-shells (larger $\delta\Phi_{AC}$).[42−44] On the other hand, the HOMO energy levels of ZnO NPs, ZnO NAs, ZNs, and ZNLs were determined at −7.39, −7.18, −7.16, and −7.13 eV, respectively. Combining with the data of optical band gaps (E_g) of ZnO NPs, ZnO NAs, ZNs, and ZNLs, which were displayed with the values as 3.14 eV, 3.13 eV, 3.04 and 2.92 eV respectively, in Figure 6. And the detailed calculation of E_g was exhibited in the Supporting Information. The LUMO energies of ZnO NPs, ZnO NAs, ZNs, and ZNLs were −4.25, −4.05, −4.12, and −4.21 eV. The various energy levels of the devices revealed the different band alignment of i-PSCs with ZnO NPs, ZnO NAs, ZNs, and ZNLs as ETLs. The considerable reduction in WF, well energy band alignment of device's structure and interfacial dipole effect of ZNs and ZNLs films, resulting from the polar small molecules, could greatly reduce the electron injection barrier and establish efficient electron−hole balance in the device.

Besides, the enhancement in photovoltaic properties was also related to the charge transport and collection. So, the impact of N719 shell and N719/LCs double-shells on carrier mobility had been assessed in i-PSCs. To measure electron mobility (μ) of the devices with ZnO NPs, ZnO NAs, ZNs, and ZNLs as ETLs, the single-carrier space charge limited conduction (SCLC)[45−47] on electron-only devices was presented in Figure S7 in the Supporting Information. Comparing to the device with pure ZnO NPs, the electron mobility of devices with ZnO NA interlayer improved from 1.28×10^{-3} cm^2 V^{-1} s^{-1} to 1.67×10^{-3} cm^2 V^{-1} s^{-1} with the length of ZnO NAs increasing to ∼50 nm (10−20 min of the growth time), and then reduced with longer ZnO NAs continuously, derived from the one-dimensional electron transport channel with high degree of order in a certain length range of ZnO NAs. In addition, after the N719 shell and N719/LCs double-shells covering onto ZnO NAs, the electron mobilities of device were further significantly boosted to 1.93×10^{-3} cm^2 V^{-1} s^{-1} and 1.78×10^{-3} cm^2 V^{-1} s^{-1}, respectively, at the length of nanoarrays with approximate 50 nm, which was because of the surface defect passivation effect of ZnO NAs with N719 shell modification and the more orderly conjugated channel of electrons' migration driven by mesogenic phase organization. Furthermore, optical transmittance spectra of ZnO NPs, ZnO NAs, ZNs, and ZNLs spin-coating onto ITO were illustrated in Figure S8 in the Supporting Information. The influence of dye absorption was not obviously observed because the thickness of N719 layer was very thin. The transmittances of ZnO NA, ZN, and ZNL ETL films were identical to that of the pristine ZnO NPs almost, and showed improving in the wavelength of 400−800 nm, revealing the light-harvesting in the active layer would not be hindered by ETLs.

With the success of ZnO NAs under the control of length nanoarrays range from 30 to 120 nm as ETL, the photovoltaic performance of devices with different thickness of ZNLs was studied and the parameters of device were plotted as a function of the thickness of ZNLs in Figure S9 in the Supporting

Information. For HTL, the MoO_3 solution was spin-casted on top of P3HT:$PC_{61}BM$ active layer, and then the film was processed with thermal annealing at 100 °C for 10 min. The MoO_3 layer with ~8 nm thickness was formed. When the thickness of ZNLs was increased, the J_{sc} and PCE of devices were first enhanced and then sloped dramatically with the thickness of ZNLs over ~50 nm, mainly deriving from the better electron mobility in a certain thickness range and the formation of direct electron transport channel of ZNLs with highly orientation. However, the V_{oc} and FF were reduced slightly and gradually, and then declined sharply upon the thickness more than 50 nm originating from the relative poor interface contact of active layer components and nanoarrays and the higher R_s and lower R_{sh} when the thickness of ETL was increasing, which were corresponded to the results of Table 1. Therefore, the length of nanoarrays could affect the performance of cells greatly and the optimal thickness of nanoarrays layer was 40−50 nm. In addition, the solution-processed device with ZNLs as ETL was also considered as a key technology toward commercialization for the environmentally friendly alcohol-soluble interlayer and solution processing of device fabrication.

Using an active layer of poly[4,8-bis(2-ethylhexyloxyl)benzo-[1,2-b:4,5-b'dithiophene-2,6-diyl-*alt*-ethylhexyl-3-uorothithieno[3,4-*b*]thiophene-2-carboxylate-4,6-diyl]] (PTB7) and [6,6]-phenyl C_{71}-butyric acid methyl ester ($PC_{71}BM$), we applied ZnO NPs, ZnO NAs, ZNs, and ZNLs as cathode interlayers with the device structure ITO/ZnO NPs, ZnO NAs, ZNs, or ZNLs/PTB7:$PC_{71}BM$/MoO_3/Ag under simulated 100 mW/cm^2 AM 1.5G illumination. To fabricate the device based on PTB7:$PC_{71}BM$, we directly deposited 8 nm MoO_3 onto the surface of active layers. Their photovoltaic characteristic values are listed in Table 1 and displayed in Figure 7. For the device with 40−50 nm thickness of nanoarrays as ETL, the prominent performances could be achieved, as the PCE increased from 6.5% (J_{sc} of 13.7 mA/cm^2, V_{oc} of 0.73 V, FF of 65%) for ZnO NPs and 6.1% (J_{sc} of 16.0 mA/cm^2, V_{oc} of 0.72 V, FF of 53%) for ZnO NAs to 7.0% (J_{sc} of 16.5 mA/cm^2, V_{oc} of 0.73 V, FF of 58%) for ZNs. Further optimization of the device with core/double-shells modification, an average PCE of 7.8% (the corresponding parameters: J_{sc} of 16.4 mA/cm^2, V_{oc} of 0.73 V, FF of 65%) could be obtained. The J_{sc} of the devices with ZnO NA, ZN, and ZNL interlayers all increased obviously from the pristine device with ZnO NPs, which might be due to the excellent optical effect and higher electron mobility of devices with inorganic nanoarrays. On the other hand, the devices with ZNs and ZNLs interlayers revealed the enhancements in J_{sc}, V_{oc}, and FF compared to the device with ZnO NA layer. The increases in J_{sc} of devices with ZNs and ZNLs were originating from the better crystal quality, fewer surface defects, better electron extraction efficiency and relative lower WF of ZNs and ZNLs with conjugated shell and double-shells modifications. The reason for higher V_{oc} was due to the excellent interfacial contact of active layer and cathode electrode, and the better energy band alignment of devices upon introduction of N719 shell or N719/LCs double-shells. Comparing the device with ZnO NPs as ETL, the FF of device with ZnO NAs decreased from 65 to 53%, resulting from the relative poor interface contact of active layer components and ZnO NAs. In addition, the excellent FF of devices with ZNs (58%) and ZNLs (65%) originated from the better interfacial contact of devices for the infiltration of PTB7:$PC_{71}BM$ molecules into ZNs and ZNLs well (see Figure S11 in the Supporting Information) after the shells' modifications and the active layer's reorganization driven by organization of LCs. To further verify the optical effect with nanoarrays on the device performance, we processed external quantum efficiency (EQE) measurements and UV−vis absorption of the cells with ZnO NP, ZnO NA, ZN, and ZNL interlayers.[48] The total absorption of active layer in the devices with ZnO NP, ZnO NA, ZN, and ZNL cathode interlayers were tested in reflection mode (Figure 7). Comparing the device with ZnO NPs, the absorption between 300 and 700 nm was enhanced in the cells with the ZnO NA, ZN, and ZNLs optical spacers for the doubled path length in the active layer as a result of reflection among the nanoarrays. The increased absorption was corresponding with the EQE spectra of Figure 7 well where the quantum efficiency enhanced to the value up to 80% between 300 and 700 nm. Due to the insertion of thicker ZnO NAs, a slight increase was demonstrated in the EQE and absorption spectra at the short wavelength around 410 nm. And, the absorption at longer wavelength, especially for the absorption peak near the active layer, improved obviously, which could result in the increase of

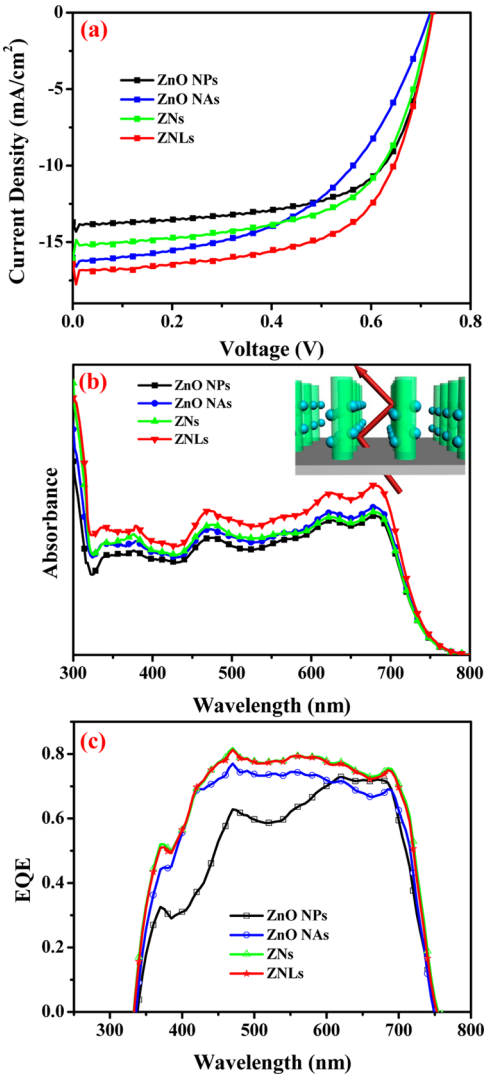

Figure 7. (a) Current density versus voltage (J−V) characteristics, (b) total absorption spectra measured in a reflection geometry, and (c) EQE spectra of the devices for inverted PSCs based on PTB7:$PC_{71}BM$ active layer with ZnO NP, ZnO NA, ZN, and ZNL interlayers.

J_{sc}. Besides, according to the characterizations of devices above, the enhancement in PCE could be mainly resulted from the additional pathway for electrons' transport created by the high coverage of N719 shell or N719/LCs double-shells on the ZnO NA surface and the promoted electron conduction on the surface. Therefore, the chance for electron/hole recombination at the D/A interface could be reduced, and cut off by forming the direct contact of conjugated small molecules (N719 and LCs) and ZnO NAs, facilitating a more effective collection of electrons from the active layer to cathode electrode.

CONCLUSIONS

ZN core/shell and ZNL core/double-shells form by an inorganic core and conformal organic double-shells as ETLs were applied in i-PSCs. Because of the low charge generation and rich amount of deep-level defects on ZnO NA surface, the N719 shell and N719/LCs double-shell modifications not only provided a direct electron transport channel but also reduced the electron extraction barrier for the lower WF and defect passivation of ZNs and ZNLs films. By controlling the length of nanoarrays layer, it was possible to improve the photovoltaic performance as our results demonstrating and the best thickness is approximate 50 nm. The devices based on PTB7:$PC_{71}BM$ active layer with ZnO NA, ZN, and ZNL interlayers showed significant enhancements in the J_{sc} value compared to device with as-prepared ZnO NPs due to the higher electron mobility and enhancement of light absorption as optical layer (optical effect). On the other hand, the liquid crystalline organization allowed the active layer components to rearrange, which could facilitate a more orderly nanomorphology of active layer and consequence reduce the chance for electron/hole recombination at the interface of D/A materials, ascribing to the presentation of direct pathway of electron and a more effective collection of electron from the active layer to cathode. Optimization of the device through controlling the thickness of nanoarrays interlayer, the average PCE of devices with ZnO NP and ZnO NA layers were 6.6% and 6.3%. After utilization of the ZN core/shell and ZNL core/double-shell layer, the devices could be further boost to the best PCE of 7.3% and 8.0%, respectively. We believe that the present findings provide novel directions for achieving high-efficiency i-PSCs using highly electron-conducting ZN and ZNL materials.

ASSOCIATED CONTENT

Supporting Information

Text giving the detailed experimental procedures and characterizations. Further analysis of the morphology change of the ZnO NAs over grown time, the optical properties of films by spin-coating active layer onto ZNs and ZNLs surface, the SCLC measurements of devices with ZnO NA, ZN, and ZNL interlayers over grown time and the photovoltaic properties of devices. This material is available free of charge via the Internet at http://pubs.acs.org/.

AUTHOR INFORMATION

Corresponding Author

*E-mail: ywchen@ncu.edu.cn. Tel.: +86 791 83969562. Fax: +86 791 83969561.

Notes

The authors declare no competing financial interest.

ACKNOWLEDGMENTS

The financial supports for this work are provided by the National Natural Science Foundation of China (51273088 and 51302130) and Doctoral Programs Foundation of Ministry of Education of China (Grants 20133601110004 and 20133601120006). Yueqin Shi and Licheng Tan contributed equally to this work.

REFERENCES

(1) Zhou, H.; Zhang, Y.; Mai, C.-K.; Collins, S. D.; Nguyen, T.-Q.; Bazan, G. C.; Heeger, A. J. Conductive Conjugated Polyelectrolyte as Hole-Transporting Layer for Organic Bulk Heterojunction Solar Cells. *Adv. Mater.* **2014**, *26*, 780−785.

(2) Yu, G.; Gao, J.; Hummelen, J. C.; Wudl, F.; Heeger, A. J. Polymer Photovoltaic Cells: Enhanced Efficiencies via a Network of Internal Donor-Acceptor Heterojunctions. *Science* **1995**, *270*, 1789−1791.

(3) Zhong, Y.; Ma, J.; Hashimoto, K.; Tajima, K. Electric Field-Induced Dipole Switching at the Donor/Acceptor Interface in Organic Solar Cells. *Adv. Mater.* **2013**, *25*, 1071−1075.

(4) Yang, T.; Wang, M.; Duan, C.; Hu, X.; Huang, L.; Peng, J.; Huang, F.; Gong, X. Inverted Polymer Solar Cells with 8.4% Efficiency by Conjugated Polyelectrolyte. *Energy Environ. Sci.* **2012**, *5*, 8208−8214.

(5) Liao, S.-H.; Jhuo, H.-J.; Cheng, Y.-S.; Chen, S.-A. Fullerene Derivative-Doped Zinc Oxide Nanofilm as the Cathode of Inverted Polymer Solar Cells with Low-Bandgap Polymer (PTB7-Th) for High Performance. *Adv. Mater.* **2013**, *25*, 4766−4771.

(6) Yoon, Y.; Kim, H. J.; Cho, C.-H.; Kim, S.; Son, H. J.; Ko, M.-J.; Kim, H.; Lee, D.-K.; Kim, J. Y.; Lee, W.; Kim, B. J.; Kim, B. Carrier Lifetime Extension via the Incorporation of Robust Hole/Electron Blocking Layers in Bulk Heterojunction Polymer Solar Cells. *ACS Appl. Mater. Interfaces* **2014**, *6*, 333−339.

(7) Zhou, Y.; Fuentes-Hernandez, C.; Shim, J.; Meyer, J.; Giordano, A. J.; Li, H.; Winget, P.; Papadopoulos, T.; Cheun, H.; Kim, J.; Fenoll, M.; Dindar, A.; Haske, W.; Najafabadi, E.; Khan, T. M.; Sojoudi, H.; Barlow, S.; Graham, S.; Brédas, J. L.; Marder, S. R.; Kahn, A.; Kippelen, B. A Universal Method to Produce Low-Work Function Electrodes for Organic Electronics. *Science* **2012**, *336*, 327−332.

(8) Kang, H.; Hong, S.; Lee, J.; Lee, K. Electrostatically Self-Assembled Nonconjugated Polyelectrolytes as an Ideal Interfacial Layer for Inverted Polymer Solar Cells. *Adv. Mater.* **2012**, *24*, 3005−3009.

(9) Cho, N.; Li, C.-Z.; Yip, H.-L.; Jen, A. K.-Y. In-Situ Doping and Crosslinking of Fullerenes to Form Efficient and Robust Electron-Transporting Layers for Polymer Solar Cells. *Energy Environ. Sci.* **2014**, *7*, 638−643.

(10) Liu, J.; Durstock, M.; Dai, L. Graphene Oxide Derivatives as Hole- and Electron-Extraction Layers for High-Performance Polymer Solar Cells. *Energy Environ. Sci.* **2014**, *7*, 1297−1306.

(11) Small, C. E.; Chen, S.; Subbiah, J.; Amb, C. M.; Tsang, S.-W.; Lai, T.-H.; Reynolds, J. R.; So, F. High-efficiency Inverted Dithienogermole-Thienopyrrolodione-Based Polymer Solar Cells. *Nat. Photonics* **2012**, *6*, 115−120.

(12) Sakohara, S.; Ishida, M. Visible Luminescence and Surface Properties of Nanosized ZnO Colloids Prepared by Hydrolyzing Zinc Acetate. *J. Phys. Chem. B* **1998**, *102*, 10169−10175.

(13) Monticone, S.; Tufeu, R.; Kanaev, A. V. Complex Nature of the UV and Visible Fluorescence of Colloidal ZnO Nanoparticles. *J. Phys. Chem. B* **1998**, *102*, 2854−2862.

(14) Park, H.; Chang, S.; Jean, J.; Cheng, J. J.; Araujo, P. T.; Wang, M.; Bawendi, M. G.; Dresselhaus, M. S.; Bulović, V.; Kong, J.; Gradečak, S. Graphene Cathode-Based ZnO Nanowire Hybrid Solar Cells. *Nano Lett.* **2013**, *13*, 233−239.

(15) Kim, J. S.; Park, Y.; Lee, D. Y.; Lee, J. H.; Park, J. H.; Kim, J. K.; Cho, K. Poly(3-hexylthiophene) Nanorods with Aligned Chain Orientation for Organic Photovoltaics. *Adv. Funct. Mater.* **2010**, *20*, 540−545.

(16) Park, S.-E.; Kim, S.; Kim, K.; Joe, H.-E.; Jung, B.; Kim, E.; Kim, W.; Min, B.-K.; Hwang, J. Fabrication of Ordered Bulk Heterojunction Organic Photovoltaic Cells using Nanopatterning and Electrohydrodynamic Spray Deposition Methods. *Nanoscale* **2012**, *4*, 7773−7779.
(17) Wallentin, J.; Anttu, N.; Asoli, D.; Huffman, M.; Åberg, I.; Magnusson, M. H.; Siefer, G.; Fuss-Kailuweit, P.; Dimroth, F.; Witzigmann, B.; Xu, H. Q.; Samuelson, L.; Deppert, K.; Borgström, M. T. InP Nanowire Array Solar Cells Achieving 13.8% Efficiency by Exceeding the Ray Optics Limit. *Science* **2013**, *339*, 1057−1060.
(18) Olson, T. Y.; Chernov, A. A.; Drabek, B. A.; Satcher, J. H., Jr.; Han, T. Y.-J. Experimental Validation of the Geometrical Selection Model for Hydrothermally Grown Zinc Oxide Nanowire Arrays. *Chem. Mater.* **2013**, *25*, 1363−1371.
(19) Vayssieres, L.; Keis, K.; Lindquist, S.-E.; Hagfeldt, A. Purpose-Built Anisotropic Metal Oxide Material: 3D Highly Oriented Microrod Array of ZnO. *J. Phys. Chem. B* **2001**, *105*, 3350−3352.
(20) Hsieh, C.-H.; Cheng, Y.-J.; Li, P.-J.; Chen, C.-H.; Dubosc, M.; Liang, R.-M.; Hsu, C.-S. Highly Efficient and Stable Inverted Polymer Solar Cells Integrated with a Cross-Linked Fullerene Material as an Interlayer. *J. Am. Chem. Soc.* **2010**, *132*, 4887−4893.
(21) Cui, Q.; Liu, C.; Wu, F.; Yue, W.; Qiu, Z.; Zhang, H.; Gao, F.; Shen, W.; Wang, M. Performance Improvement in Polymer/ZnO Nanoarray Hybrid Solar Cells by Formation of ZnO/CdS-Core/Shell Heterostructures. *J. Phys. Chem. C* **2013**, *117*, 5626−5637.
(22) Xie, C.; Nie, B.; Zeng, L.; Liang, F.-X.; Wang, M.-Z.; Luo, L.; Feng, M.; Yu, Y.; Wu, C.-Y.; Wu, Y.; Yu, S.-H. Core-Shell Heterojunction of Silicon Nanowire Arrays and Carbon Quantum Dots for Photovoltaic Devices and Self-Driven Photodetectors. *ACS Nano* **2014**, *8*, 4015−4022.
(23) Watanabe, M.; Tsuchiya, K.; Shinnai, T.; Kijima, M. Liquid Crystalline Polythiophene Bearing Phenylnaphthalene Side-Chain. *Macromolecules* **2012**, *45*, 1825−1832.
(24) Deshmukh, P.; Ahn, S.-K.; Merxem, L. G. D.; Kasi, R. M. Interplay between Liquid Crystalline Order and Microphase Segregation on the Self-Assembly of Side-Chain Liquid Crystalline Brush Block Copolymers. *Macromolecules* **2013**, *46*, 8245−8252.
(25) Shin, W.; Yasuda, T.; Watanabe, G.; Yang, Y. S.; Adachi, C. Self-Organizing Mesomorphic Diketopyrrolopyrrole Derivatives for Efficient Solution-Processed Organic Solar Cells. *Chem. Mater.* **2013**, *25*, 2549−2556.
(26) Chen, L.-M.; Hong, Z.; Li, G.; Yang, Y. Recent Progress in Polymer Solar Cells: Manipulation of Polymer:Fullerene Morphology and the Formation of Efficient Inverted Polymer Solar Cells. *Adv. Mater.* **2009**, *21*, 1434−1449.
(27) Chang, J. A.; Im, S. H.; Lee, Y. H.; Kim, H.-J.; Lim, C.-S.; Heo, J. H.; Seok, S. Panchromatic Photon-Harvesting by Hole-Conducting Materials in Inorganic-Organic Heterojunction Sensitized-Solar Cell through the Formation of Nanostructured Electron Channels. *Nano Lett.* **2012**, *12*, 1863−1867.
(28) Selinsky, R. S.; Ding, Q.; Faber, M. S.; Wright, J. C.; Jin, S. Quantum Dot Nanoscale Heterostructures for Solar Energy Conversion. *Chem. Soc. Rev.* **2013**, *42*, 2963−2985.
(29) Li, F.; Shi, Y.; Yuan, K.; Chen, Y. Fine Dispersion and Self-assembly of ZnO Nanoparticles Driven by P3HT-b-PEO Diblocks for Improvement of Hybrid Solar Cells Performance. *New J. Chem.* **2013**, *37*, 195−203.
(30) Lin, Y.-H.; Faber, H.; Zhao, K.; Wang, Q.; Amassian, A.; McLachlan, M.; Anthopoulos, T. D. High-Performance ZnO Transistors Processed Via an Aqueous Carbon-Free Metal Oxide Precursor Route at Temperatures Between 80−180 °C. *Adv. Mater.* **2013**, *25*, 4340−4346.
(31) Yu, X.; Xiao, K.; Chen, J.; Lavrik, N. V.; Hong, K.; Sumpter, B. G.; Geohegan, D. B. High-Performance Field-Effect Transistors Based on Polystyrene-*b*-Poly(3-hexylthiophene) Diblock Copolymers. *ACS Nano* **2011**, *5*, 3559−3567.
(32) Borchert, H. Elementary Processes and Limiting Factors in Hybrid Polymer/Nanoparticle Solar Cells. *Energy Environ. Sci.* **2010**, *3*, 1682−1694.
(33) Reiss, P.; Couderc, E.; Girolamo, J. D.; Pron, A. Conjugated Polymers/Semiconductor Nanocrystals Hybrid Materials-Preparation, Electrical Transport Properties and Applications. *Nanoscale* **2011**, *3*, 466−489.
(34) Moulé, A. J.; Chang, L.; Thambidurai, C.; Vidu, R.; Stroeve, P. Hybrid Solar Cells: Basic Principles and the Role of Ligands. *J. Mater. Chem.* **2012**, *22*, 2351−2368.
(35) Shi, Y.; Tan, L.; Chen, L.; Chen, Y. In Situ Fabricating One-Dimensional Donor-Acceptor Core-Shell Hybrid Nanobeams Network Driven by Self-Assembly of Diblock Copolythiophenes. *Macromolecules* **2014**, *47*, 1757−1767.
(36) Shi, Y.; Li, F.; Tan, L.; Chen, Y. Hybrid Bulk Heterojunction Solar Cells Based on the Cooperative Interaction of Liquid Crystals within Quantum Dots and Diblock Copolymers. *ACS Appl. Mater. Interfaces* **2013**, *5*, 11692−11702.
(37) Brabec, C. J.; Heeney, M.; McCulloch, I.; Nelson, J. Influence of Blend Microstructure on Bulk Heterojunction Organic Photovoltaic Performance. *Chem. Soc. Rev.* **2011**, *40*, 1185−1199.
(38) Treat, N. D.; Varotto, A.; Takacs, C. J.; Batara, N.; Al-Hashimi, M.; Heeney, M. J.; Heeger, A. J.; Wudl, F.; Hawker, C. J.; Chabinyc, M. L. Polymer-Fullerene Miscibility: A Metric for Screening New Materials for High-Performance Organic Solar Cells. *J. Am. Chem. Soc.* **2012**, *134*, 15869−15879.
(39) Kim, Y.-H.; Han, T.-H.; Cho, H.; Min, S.-Y.; Lee, C.-L.; Lee, T.-W. Polyethylene Imine as an Ideal Interlayer for Highly Efficient Inverted Polymer Light-Emitting Diodes. *Adv. Funct. Mater.* **2014**, *24*, 3808−3814.
(40) Lim, D. C.; Kim, K.-D.; Park, S.-Y.; Hong, E. M.; Seo, H. O.; Lim, J. H.; Lee, K. H.; Jeong, Y.; Song, C.; Lee, E.; Kim, Y. D.; Cho, S. Towards Fabrication of High-Performing Organic Photovoltaics: New Donor Polymer, Atomic Layer Deposited Thin Buffer Layer and Plasmonic Effects. *Energy Environ. Sci.* **2012**, *5*, 9803−9807.
(41) Page, Z. A.; Duzhko, V. V.; Emrick, T. Conjugated Thiophene-Containing Polymer Zwitterions: Direct Synthesis and Thin Film Electronic Properties. *Macromolecules* **2013**, *46*, 344−351.
(42) Seo, J. H.; Gutacker, A.; Sun, Y.; Wu, H.; Huang, F.; Cao, Y.; Scherf, U.; Heeger, A. J.; Bazan, G. C. Improved High-Efficiency Organic Solar Cells via Incorporation of a Conjugated Polyelectrolyte Interlayer. *J. Am. Chem. Soc.* **2011**, *133*, 8416−8419.
(43) Scharber, M. C.; Mühlbacher, D.; Koppe, M.; Denk, P.; Waldauf, C.; Heeger, A. J.; Brabec, C. J. Design Rules for Donors in Bulk-Heterojunction Solar Cells-Towards 10% Energy-Conversion Efficiency. *Adv. Mater.* **2006**, *18*, 789−794.
(44) He, C.; Zhong, C.; Wu, H.; Yang, R.; Yang, W.; Huang, F.; Bazan, G. C.; Cao, Y. Origin of the Enhanced Open-Circuit Voltage in Polymer Solar Cells *via* Interfacial Modification using Conjugated Polyelectrolytes. *J. Mater. Chem.* **2010**, *20*, 2617−2622.
(45) Mihailetchi, V. D.; van Duren, J. K. J.; Blom, P. W. M.; Hummelen, J. C.; Janssen, R. A. J.; Kroon, J. M.; Rispens, M. T.; Verhees, W. J. H.; Wienk, M. M. Electron Transport in a Methanofullerene. *Adv. Funct. Mater.* **2003**, *13*, 43−46.
(46) Melzer, C.; Koop, E. J.; Mihailetchi, V. D.; Blom, P. W. M. Hole Transport in Poly(phenylene vinylene)/Methanofullerene Bulk-Heterojunction Solar Cells. *Adv. Funct. Mater.* **2004**, *14*, 865−870.
(47) Koster, L. J. A.; van Strien, W. J.; Beek, W. J. E.; Blom, P. W. M. Device Operation of Conjugated Polymer/Zinc Oxide Bulk Heterojunction Solar Cells. *Adv. Funct. Mater.* **2007**, *17*, 1297−1302.
(48) Kyaw, A. K. K.; Wang, D. H.; Wynands, D.; Zhang, J.; Nguyen, T.-Q.; Bazan, G. C.; Heeger, A. J. Improved Light Harvesting and Improved Efficiency by Insertion of an Optical Spacer (ZnO) in Solution-Processed Small-Molecule Solar Cells. *Nano Lett.* **2013**, *13*, 3796−3801.